Calculations of High-Temperature Jet Flow Using Hybrid Reynolds-Averaged Navier–Stokes Formulations

Khaled S. Abdol-Hamid*
NASA Langley Research Center, Hampton, Virginia 23681
and
Alaa Elmiligui†
Analytical Services & Materials, Inc., Hampton, Virginia 23666

Two multiscale-type turbulence models are implemented in the PAB3D solver. The models are based on modifying the Reynolds-averaged Navier–Stokes equations. The first scheme is a hybrid Reynolds-averaged-Navier–Stokes/large-eddy-simulation model using the two-equation $k\varepsilon$ model with a Reynolds-averaged-Navier–Stokes/large-eddy-simulation transition function dependent on grid spacing and the computed turbulence length scale. The second scheme is a modified version of the partially averaged Navier–Stokes model in which the unresolved kinetic energy parameter f_k is allowed to vary as a function of grid spacing and the turbulence length scale. This parameter is estimated based on a novel two-stage procedure to efficiently estimate the level of scale resolution possible for a given flow on a given grid for partially averaged Navier–Stokes. It has been found that the prescribed scale resolution can play a major role in obtaining accurate flow solutions. The parameter f_k varies between zero and one and is equal to one in the viscous sublayer and when the Reynolds-averaged Navier–Stokes turbulent viscosity becomes smaller than the large-eddy-simulation viscosity. The formulation, usage methodology, and validation examples are presented to demonstrate the enhancement of PAB3D's time-accurate turbulence modeling capabilities. The accurate simulations of flow and turbulent quantities will provide a valuable tool for accurate jet noise predictions. Solutions from these models are compared with Reynolds-averaged Navier–Stokes results and experimental data for high-temperature jet flows. The current results show promise for the capability of hybrid Reynolds-averaged Navier–Stokes and large eddy simulation and partially averaged Navier–Stokes in simulating such flow phenomena.

I. Introduction

THE limited capability of the Reynolds-averaged Navier–Stokes (RANS) approach, combined with eddy-viscosity turbulence models to simulate unsteady and complex flows, has been known for some time. The RANS assumption is that most of the energy is modeled through the turbulence transport equations and is resolved in the grid. RANS overpredicts the eddy viscosity, which results in excessive damping of unsteady motion. Consequently, the eddy viscosity attains unphysically large values due to unresolved scales and suppresses most temporal and spatial fluctuations in the resolved flowfield. One of the approaches used to overcome this problem is to provide a mechanism for the RANS equations to resolve the largest scales of motion. Among several methods, the detached eddy simulations (DES) [1], the hybrid large eddy simulation (LES) [2,3], the limited numerical scheme (LNS) [4], and the partially averaged Navier–Stokes (PANS) [5] provide the mechanisms needed to satisfy this requirement.

In an attempt to increase the fidelity and accuracy of the PAB3D code‡ [6,7], a hybrid turbulence model RANS/LES [2,3] and PANS [8] have been added. Abdol-Hamid and Girimaji [8] explored a new approach to improve the accuracy and robustness of PANS in creating a simulation of an unsteady flowfield. They accomplished this through the development and implementation of a two-stage procedure to efficiently estimate the level of scale resolution possible for a given flow on a given grid for PANS and other hybrid models. This capability was implemented in a general applied aerodynamics computational fluid dynamics (CFD) research code, PAB3D, for the simulation of unsteady flows.

Both large temperature and pressure fluctuations have a profound effect on turbulence. Although several models have been developed to account for the effect of pressure fluctuations (compressibility correction models), very little has been done to account for large temperature fluctuations. This has led to poor CFD prediction of nonisothermal flows. For high-temperature jet flow, the standard turbulence models lack the ability to predict the observed increase in growth rate of the mixing layer [9,10]. Several researchers [11–16] have modified one or more terms of the transport equations to obtain better agreement in high-temperature flows. These modifications directly or indirectly affect the closure terms of the turbulent heat flux $\overline{\rho u_i \theta}$ and stresses $\rho \overline{u_i u_j}$. Theis and Tam [11] changed several coefficients in the turbulent transport equations. However, such extensive modifications of model coefficients completely change the characteristics of the equations and may cause deficiencies in flow prediction accuracy for other problems. Other attempts to sensitize the turbulence model to temperature fluctuations involve more sophisticated closure for the turbulent heat flux term appearing in the average energy equation [14–16]. Explicit algebraic nonlinear heat flux models have also been tested for this purpose. These models have been successful in some fully developed high-temperature turbulent flows. A simpler approach was to model the value of C_μ as a function of the total temperature gradient in the flow [17]. The concept behind this approach was to postulate that the large-scale density nonuniformity in the flow would introduce local mixing instability and added turbulence stresses. The modification in [17] was successful in predicting the hot-jet mixing rate over a wide range of temperature ratios between the jet and the ambient air. The authors

‡Data available online at http://www.asm-usa.com/PAB3D [retrieved 15 October 2007].

of this paper thought that this variable C_μ would not be necessary in the multiscale turbulence model approach because the computations in the code would automatically take care of the large-scale density gradient effect.

II. Approaches

The governing equations of the time-averaged formulation include the conservation equations for mass, momentum, and energy and the equation of state. In the present study, the perfect gas law was chosen to represent the air properties, and the eddy-viscosity concept was used to model the Reynolds stresses. The mass, momentum, and energy conservation equations of the time-averaged equations can be written in a conservative form as follows:

$$\frac{\partial \rho}{\partial t} + \frac{\partial \rho u_i}{\partial x_i} = 0$$

$$\frac{\partial \rho u_i}{\partial t} + \frac{\partial (\rho u_i u_j + p \delta_{ij})}{\partial x_j} = \frac{\partial (\tau_{ij} - \rho \overline{u_i u_j})}{\partial x_j}$$

$$\frac{\partial \rho e_0}{\partial t} + \frac{\partial (\rho e_0 u_i + p u_i)}{\partial x_i} = \frac{\partial (\tau_{ij} u_j - \rho \overline{u_i u_j} u_j)}{\partial x_i} - \frac{\partial (q_i + C_P \rho \overline{u_i \theta})}{\partial x_i}$$

$$+ \frac{\partial}{\partial x_i}\left[\rho\left(\nu_l + \frac{\nu_t}{\bar{\sigma}_k}\right)\frac{\partial k}{\partial x_i}\right] \tag{1}$$

In the case of RANS equations, a standard turbulence model (STM) such as the two-equation $k\varepsilon$ turbulence model is used:

$$\frac{\partial \rho k}{\partial t} + \frac{\partial \rho u_j k}{\partial x_j} = -\rho \overline{u_j u_i}\frac{\partial u_i}{\partial x_j} + \frac{\partial}{\partial x_j}\left[\rho\left(\nu_l + \frac{c_\mu k^2}{\bar{\sigma}_k \varepsilon}\right)\frac{\partial k}{\partial x_j}\right] - \rho\varepsilon\frac{\partial \rho \varepsilon}{\partial t}$$

$$+ \frac{\partial \rho u_j \varepsilon}{\partial x_j} = -C_{\varepsilon 1}\rho\overline{u_j u_i}\frac{\partial u_i}{\partial x_j}\frac{\varepsilon}{k} + \frac{\partial}{\partial x_j}\left[\rho\left(\nu_l + \frac{c_\mu k^2}{\bar{\sigma}_\varepsilon \varepsilon}\right)\frac{\partial \varepsilon}{\partial x_j}\right]$$

$$- f_2 \tilde{C}_{\varepsilon 2}\rho\frac{\varepsilon}{k}\left[\varepsilon - \nu_l\left(\frac{\partial \sqrt{k}}{\partial x_j}\right)^2\right]C_\mu = .09$$

$$C_{\varepsilon 1} = 1.44 \qquad \bar{\sigma}_k = \sigma_k = 1.4 \qquad \bar{\sigma}_\varepsilon = \sigma_\varepsilon = 1$$

$$\overline{C_{\varepsilon 2}} = C_{\varepsilon 2} = 1.92 \qquad f_\mu = \exp\left[\frac{-3.41}{[1 + (R_T/50)]^2}\right]$$

$$R_T = \frac{k^2}{\nu_t \varepsilon} \qquad f_2 = 1. - 0.3\exp(-R_T^2) \tag{2}$$

The boundary conditions with n as the wall distance for ε and k at the wall are

$$\varepsilon_{\text{wall}} = \nu_l\left(\frac{\partial \sqrt{k}}{\partial n}\right)^2 \qquad k_{\text{wall}} = 0$$

In the present paper, we use the simple eddy diffusivity (SED) approach, which is based on the Boussinesq viscosity model. This approach is used to model all the scalar diffusion terms appearing in the RANS and standard $k\varepsilon$ equations. For the heat flux term, the SED is written as follows:

$$\rho\overline{u_i \theta} = -\frac{\rho \nu_t}{\sigma_\tau}\frac{\partial T}{\partial x_i} \qquad \sigma_\tau = 0.9$$

The turbulent stress components were formulated as

$$\rho\overline{u_j u_i} = 2\rho\nu_t S_{ji} - \frac{2}{3}\delta_{ji}\rho k \qquad S_{ji} = \frac{1}{2}\left[\frac{\partial u_j}{\partial x_i} + \frac{\partial u_i}{\partial x_j}\right] - \frac{1}{3}\delta_{ji}\frac{\partial u_k}{\partial x_k} \tag{3}$$

For the purpose of this paper, the RANS turbulent viscosity was defined as

$$\nu_t^{\text{RANS}} = f_\mu C_\mu \frac{k^2}{\varepsilon} \tag{4}$$

A. Two-Stage PANS Approach

The PANS model [5] was developed to overcome the grid dependency associated with the use of other hybrid turbulence models (HTM). In its original form, PANS [5] replaced the two-equation turbulence model by solving for the unresolved kinetic energy k_u and the dissipation ε_u. The k_u equation is identical to the original k equation. In the ε equation (2), the following coefficients were used to change the two-equation model to the HTM, which becomes known as the PANS formulation through the following changes:

$$\tilde{C}_{\varepsilon 2} = \frac{f_k}{f_\varepsilon}(C_{\varepsilon 2} - C_{\varepsilon 1}) + C_{\varepsilon 1} \qquad \bar{\sigma}_k = \frac{f_k^2}{f_\varepsilon}\sigma_k \qquad \bar{\sigma}_\varepsilon = \frac{f_k^2}{f_\varepsilon}\sigma_\varepsilon \tag{5}$$

where

$$f_k = \frac{k_u}{k} \qquad f_\varepsilon = \frac{\varepsilon_u}{\varepsilon}$$

represent the ratios of the unresolved kinetic energy and dissipation to the total kinetic energy and dissipation, respectively. It was only natural to use f_k and f_ε to quantify the PANS filter with respect to RANS. Therefore, f_k and f_ε are used as the resolution control parameters for PANS. The physics of turbulence dictates that

$$\text{(DNS)} \ 0 \leq f_k \leq f_\varepsilon \leq 1 \ \text{(RANS)}$$

The original formulation [5] used constant values for the unresolved kinetic energy parameter f_k and unresolved dissipation rate parameter f_ε. The users will select values for these parameters and refine the grid until the flow solution converges toward a solution target. This could be very time-consuming for resolving complex three-dimensional flows. In the present paper, we will discuss an approach to define the unresolved kinetic energy parameter. Abdol-Hamid and Girimaji [8] introduced a two-stage approach to estimate the values of the unresolved kinetic energy parameter. Here, we will highlight the basic concepts of this approach. Based on a simple dimension analysis, we assume that the turbulent viscosity may be related to the total kinetic energy k, ε, S, and Δ as

$$\nu_t \approx \frac{k^2}{\varepsilon} \approx \Delta^2 S \approx \Delta^2\frac{\varepsilon}{k} \tag{6}$$

which leads to

$$f_k^3 k^3 \approx \Delta^2\frac{k^3}{L^2} \tag{7}$$

Hence,

$$f_k = C_h\left[\frac{1}{\lambda}\right]^{2/3} \qquad \lambda = \frac{L}{\Delta} \qquad L = \frac{k^{3/2}}{\varepsilon} \tag{8}$$

C_h is a model coefficient, which needs to be calibrated. In the present paper, a value of 1 will be used to evaluate the model. Here, we summarize the guidelines to be followed for the sequential two-stage procedure. These guidelines are completely dependent upon flow complexity. For the first stage,

1) Complete a three-dimensional or two-dimensional simulation.
2) Use unsteady or steady calculation; high-order schemes are not required.
3) Choose a desired level of an allowable RANS turbulence model (one-equation, two-equation, algebraic stress, full Reynolds stress, etc.).

For the second stage,

1) Conduct a three-dimensional simulation.
2) Use unsteady calculation; high-order schemes should be considered.
3) Use hybrid models (DES, Hybrid RANS/LES, PANS, etc.).

The users need to use the same flow conditions, boundary conditions, and grid resolution for both stages of the procedure.

B. Hybrid RANS/LES Approach

Nichols and Nelson gave an example of a hybrid RANS/LES turbulence model. This method was implemented in conjunction with Menter's SST two-equation turbulence model and was termed a multiscale (MS) model. In the present paper, this hybrid model is used with the two-equation model described in Eqs. (2) and (3). The turbulent length scale used in this implementation was defined as

$$l_t = \max\left(6\sqrt{\frac{\nu_t^{\text{RANS}}}{\Omega}}, \ \frac{k^{3/2}}{\varepsilon}\right) \qquad \Omega_{ji} = \frac{1}{2}\left[\frac{\partial u_j}{\partial x_i} - \frac{\partial u_i}{\partial x_j}\right] \qquad (9)$$

The subgrid turbulent kinetic energy was defined as

$$k^{\text{LES}} = f_d k \qquad (10)$$

The damping function was defined as

$$f_d = \{1 + \tanh[2\pi(\Lambda - 0.5)]\}/2 \qquad (11)$$

where

$$\Lambda = \frac{1}{1 + [l_t/\Delta]^{4/3}} = \frac{1}{1 + \lambda^{4/3}} \qquad (12)$$

λ is the unresolved characteristic ratio, and

$$\Delta = \max(\Delta_x, \Delta_y, \Delta_z) \qquad (13)$$

The eddy viscosity was then calculated from

$$\nu_t = f_d \nu_t^{\text{RANS}} + (1 - f_d)\nu_t^{\text{LES}} \qquad (14)$$

$$\nu_t^{\text{LES}} = \min(\nu_t^{\text{RANS}}, \ 0.084\Delta\sqrt{k^{\text{LES}}}) \qquad (15)$$

Note that this hybrid model allowed the transition from RANS to LES as a function of the local grid spacing and the local turbulent length scale predicted by the RANS model rather than as a function of the grid spacing alone. This allowed the model to detect whether it can resolve the turbulent scales present on the existing grid before its transition over to the LES mode.

III. Results and Discussions

Two test cases were selected to evaluate the present modifications. The first test case is a single subsonic jet operated at the design pressure condition. We selected this case to compare RANS, PANS, and LES approaches in simulating subsonic jet. This case provided the calibration of the PANS approach. The second test case is a multistream subsonic jet configuration. This case addressed the complexity of modeling multistream flows. We used a 0.03 time step based on the radius of the nozzle and the freestream acoustic speed. We ran 4000 iterations to initiate the unsteadiness of the jet flow. Then the solutions were averaged over the last 20,000 iterations. It was observed that approximately four subiterations per physical time step produced the optimal convergence per iteration. However, the physics of the specific problem will dictate the subiteration number for other cases. In the present results, four subiterations typically reduced the residual by two orders of magnitude at that time level, with no improvement using more iterations.

A. High-Temperature Single Nozzle Jet Flow

The present study used the benchmark experiments performed by Bridges and Brown [18] at the NASA Glenn Laboratory with the flow condition as indicated in Table 1 for the core and freestream.

Table 1 Experimental subsonic condition

	T_t, °R	P_t, psi	M
Core	1400	17.68	0.55
Freestream	540	14.3	0.01

a) Unresolved turbulent kinetic energy parameter, f_k contours
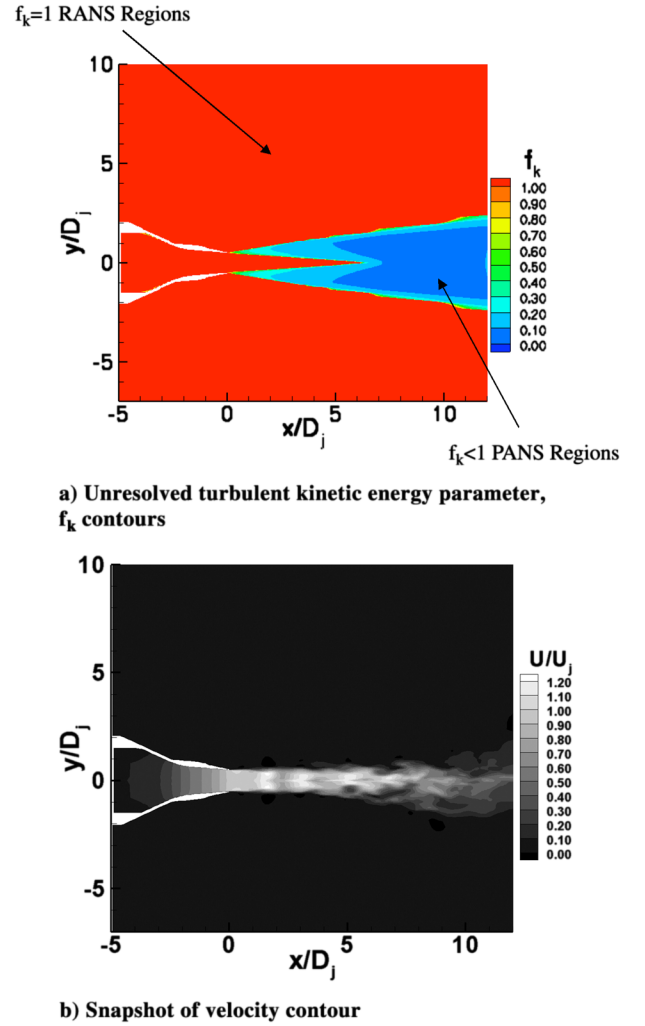

b) Snapshot of velocity contour

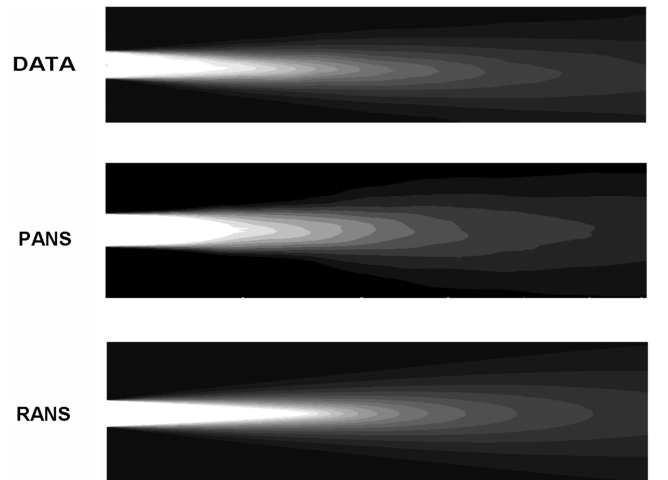Fig. 1 Single-nozzle predictions using PANS formulation.

Fig. 2 Two-dimensional time-averaged velocity contour results from RANS, and PANS formulations compared with experimental data.

The computational mesh is a full three-dimensional grid with 120 cells in the circumferential direction. The computational domain is divided into 48 blocks. The superfine mesh had a total of 4,000,000 cells. Grid points are clustered near the solid surfaces and around the shear layer. We used a uniform streamwise grid spacing for $2 < x/Dj < 12$. The value of y^+ for the first cell off the surface varied between 0.2 and 2. During the course of simulating this case,
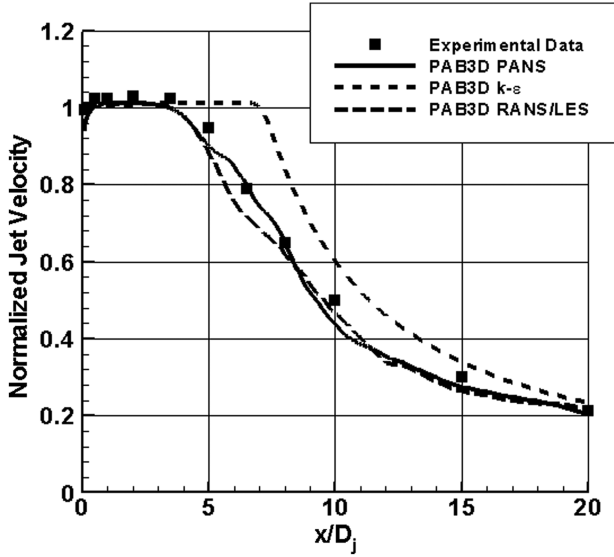
Fig. 3   Normalized jet centerline velocity results using RANS, RANS/LES, and PANS formulations compared with experimental data.
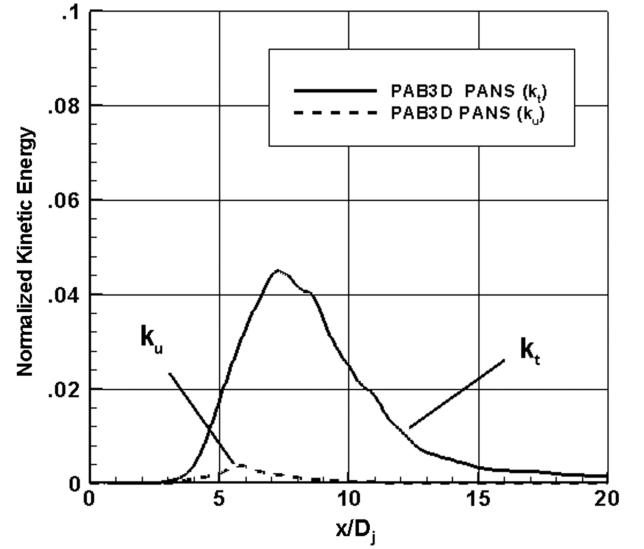

Fig. 5   Normalized unresolved turbulent kinetic energy k_u compared with total kinetic energy k_t using PANS.
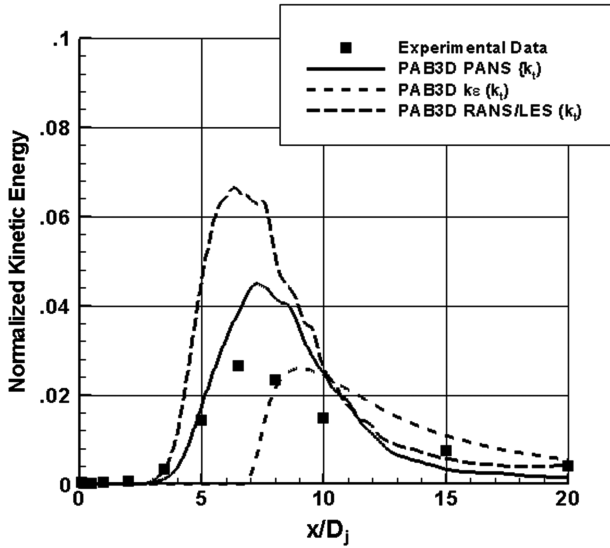

Fig. 4   Normalized jet centerline turbulent kinetic energy results using RANS, RANS/LES, and PANS formulations compared with experimental data.
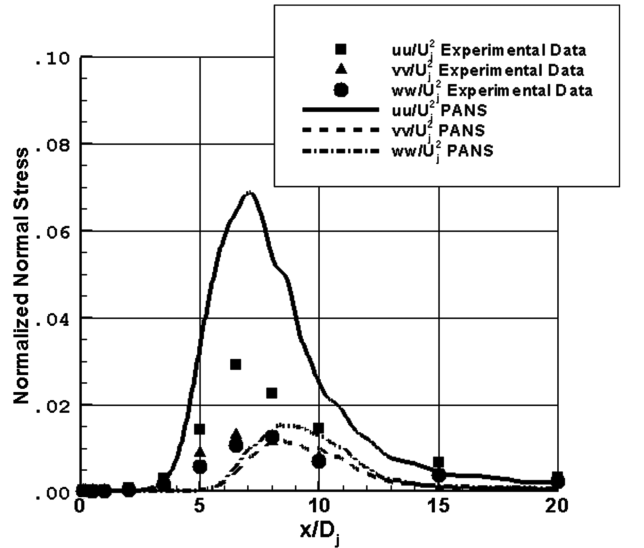

Fig. 6   Normalized normal stress components (uu, vv, and ww) compared experimental data.

we tried single- and double-precision calculations. We found no significant differences in the results. Also, we tried 4, 8, and 12 subiterations for the dual-step time-accurate approach. We also found no significant differences in the results. Based on these results, we will use single precision and four subiterations in all of the presented results in this paper.

First, we used the RANS formulation to get time-averaged quantities to calculate the characteristic length-scale ratio. This ratio varies in space and is used to produce the unresolved kinetic energy parameter f_k. Figure 1a shows the distribution of this function. This parameter identifies the RANS and PANS regions. The RANS regions are defined with the parameter set at a value of 1. The PANS regions are the remaining flow domains in which f_k values are less than one. We use this parameter in solving the PANS formulation. We calibrate the medium grid (1,000,000 cells) to get the velocity profile to closely resemble the experimental data for the velocity distribution. We found that C_h should be 1.05 for the present test case. All the calculations performed hereafter used the same value of $C_h = 1.05$.

Figure 1b shows the snapshot of a two-dimensional contour on the $X–Y$ plane for the velocity u/Uj using the PANS formulation. The

result shows the unsteady behavior of the jet flow as it interacts with the external flow. A similar observation was found as the RANS/LES formulation was used. In the RANS prediction, there was not a significant difference between the snapshot and the time-averaged flow quantities. In this case, the snapshot solution is similar to that shown in Fig. 2. This was caused by the fact that RANS overpredicts the eddy viscosity, resulting in excessive damping of unsteady motion. Consequently, the eddy viscosity attains unphysically large values due to unresolved scales, and suppresses most temporal and spatial fluctuations in the resolved flowfield.

Figure 2 shows the two-dimensional slice of the time-averaged results of using RANS and PANS formulations compared with experimental data. There were no significant differences between the time-averaged and the snapshot of the unsteady RANS result. The PANS results and similarly RANS/LES (not shown) produce a good comparison with experimental data. Figure 3 shows a comparison of the jet centerline velocity using RANS, RANS/LES, and PANS formulations compared with experimental data. Both RANS/LES and PANS produced better results compared with the RANS solution. Figure 4 shows the jet centerline turbulent kinetic energy. Both PANS and RANS/LES overpredict the total turbulent kinetic energy. We define total kinetic energy k_t as

Table 2 Experimental subsonic condition[a]

	T_t, °R	P_t, psi	M
Core	1498	21.72	0.8
Fan	647	24.36	0.9
Freestream	530	14.7	0.28

[a]Please compute the Mach numbers for the core and fan.

$$k_t = k_r + k_u = \tfrac{1}{2}[\overline{u_i u_i} - \overline{u_i}\,\overline{u_i}] + k_u$$

In the case of the RANS results, the resolved kinetic energy k_r is zero. Both RANS/LES and PANS provided a mechanism for the RANS equations to resolve the largest scales of motion. Figure 5 shows the reduction of the unresolved kinetic energy k_u compared with the total value. In general, the RANS produces the same values for all three normal stress components. Figure 6 shows the comparisons and distributions of the normal stress components (uu, vv, and ww) using PANS. In this case, PANS produced different values for the three normal stress components with a trend similar to
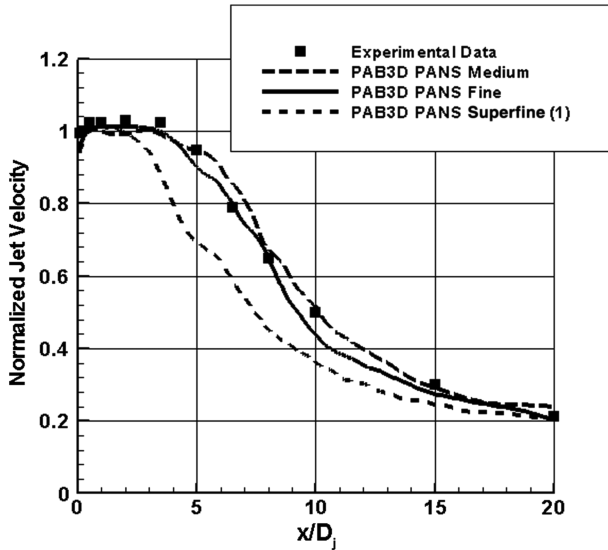
the experimental data. The levels of the vv and ww components are very close to the experimental data. The predicted uu component is much higher than the experimental data. DeBonis [19] reported the similar observation that the LES simulation produced a much higher value of uu compared with $M = 0.9$ hot-jet experimental data.

We attempted to provide a grid convergence study for the single-jet case. We tried three grid levels: 1,000,000 cells (medium), 2,000,000 cells (fine), and 4,000,000 cells (superfine). In this case, the grid was refined in the flow direction while holding the filter coefficient C_h [see Eq. (8)] constant. This causes the filter width to be refined along with the grid. The smallest value of f_k was around 0.1. Under such a procedure, the solution converged to a DNS because the filter width approaches zero along with the grid spacing. As a result, this approach attempts to calculate different turbulent scales explicitly, whether or not the numerical resolution was sufficient to accurately compute those scales. The result of this study was shown in Fig. 6. The medium and fine grids provided reasonable grid convergence. However, the superfine grid completely diverged from the other solutions, as shown in Fig. 7. This was due to limitations of

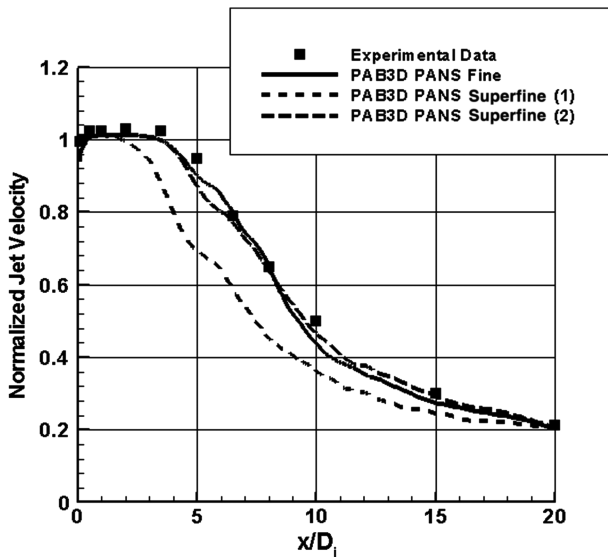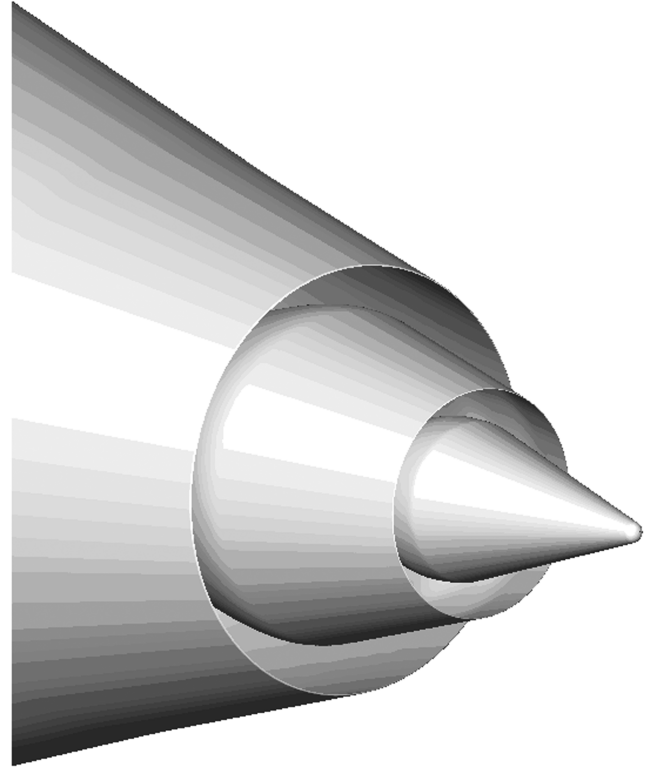**Fig. 7 Normalized jet centerline velocity results using PANS formulation compared with experimental data.**

Fig. 9 Configuration 1 baseline round core nozzle with fan nozzle.

Fig. 8 Normalized jet centerline velocity results using PANS formulation compared with experimental data.
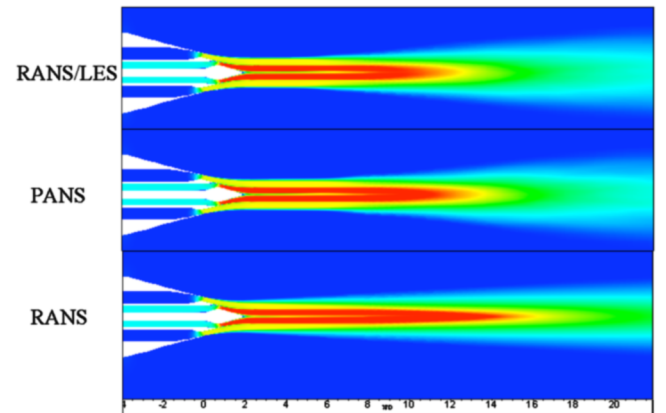

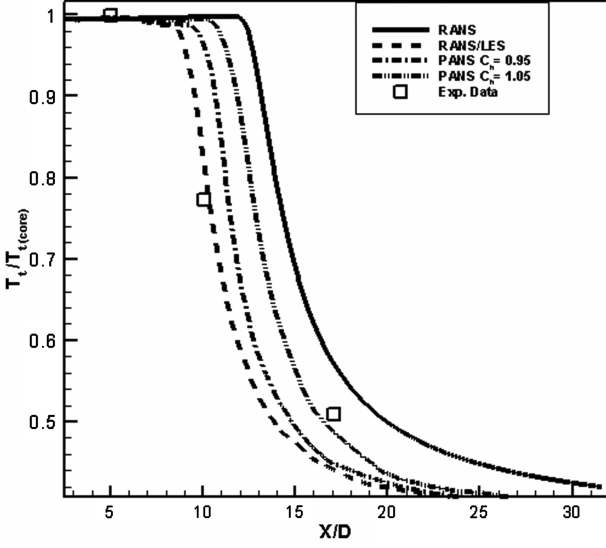**Fig. 10 Velocity contours on symmetry plane.**

Fig. 11 Comparisons of computed normalized centerline stagnation temperature and data [10].

the numerical scheme to handle such flow physics. In such a case, a higher-order scheme could be more effective. Now we freeze the value of f_k from the fine-grid solution used for the superfine grid. Figure 8 shows the comparisons of this approach with fine and superfine grids. The result of this approach improves the superfine-grid solution and now it matches the fine-grid solution. This equivalent is to use f_ε of value 0.85 instead of 1.0.

B. High-Temperature Multistream Nozzle Jet Flow

The second test configuration includes a separate fan and core nozzle flows at a bypass ratio of five with an external plug. One set of data was selected from the reported test results [20], with the flow condition as indicated in Table 2 for the core, fan, and freestream.

This test configuration was part of a comprehensive investigation on jet exhaust noise due to the pylon–chevron–jet interaction [10], which was tested at NASA. As previously discussed, the present PANS approach was tuned on the axisymmetric grid to the round nozzle experimental results. For the limited space and scope of this paper, we will discuss the comparison with only the axisymmetric configuration shown in Fig. 9.

The computational domain for the solution extended from $x/D_c = -6.3$ to 31.6 in the axial direction and $6.3D_c$ in the radial direction, where D_c is the diameter of the baseline core nozzle, 12.80 cm. The origin, $x/D_c = 0.0$, was set at the exit of the fan nozzle so that the exit of the core nozzle was at about $x/D_c = 0.5$. The computational mesh is a three-dimensional-shaped grid with 120 cells in the circumferential direction. The computational domain is divided into 92 blocks. The mesh had a total of 7,750,000 cells. Grid points are clustered near the solid surfaces and around the shear layer. The value of y^+ for the first cell off the surface varied between 0.16 and 1.8.

Computational solutions were obtained for RANS, hybrid RANS/LES, and PANS formulations. The simulated conditions were set to
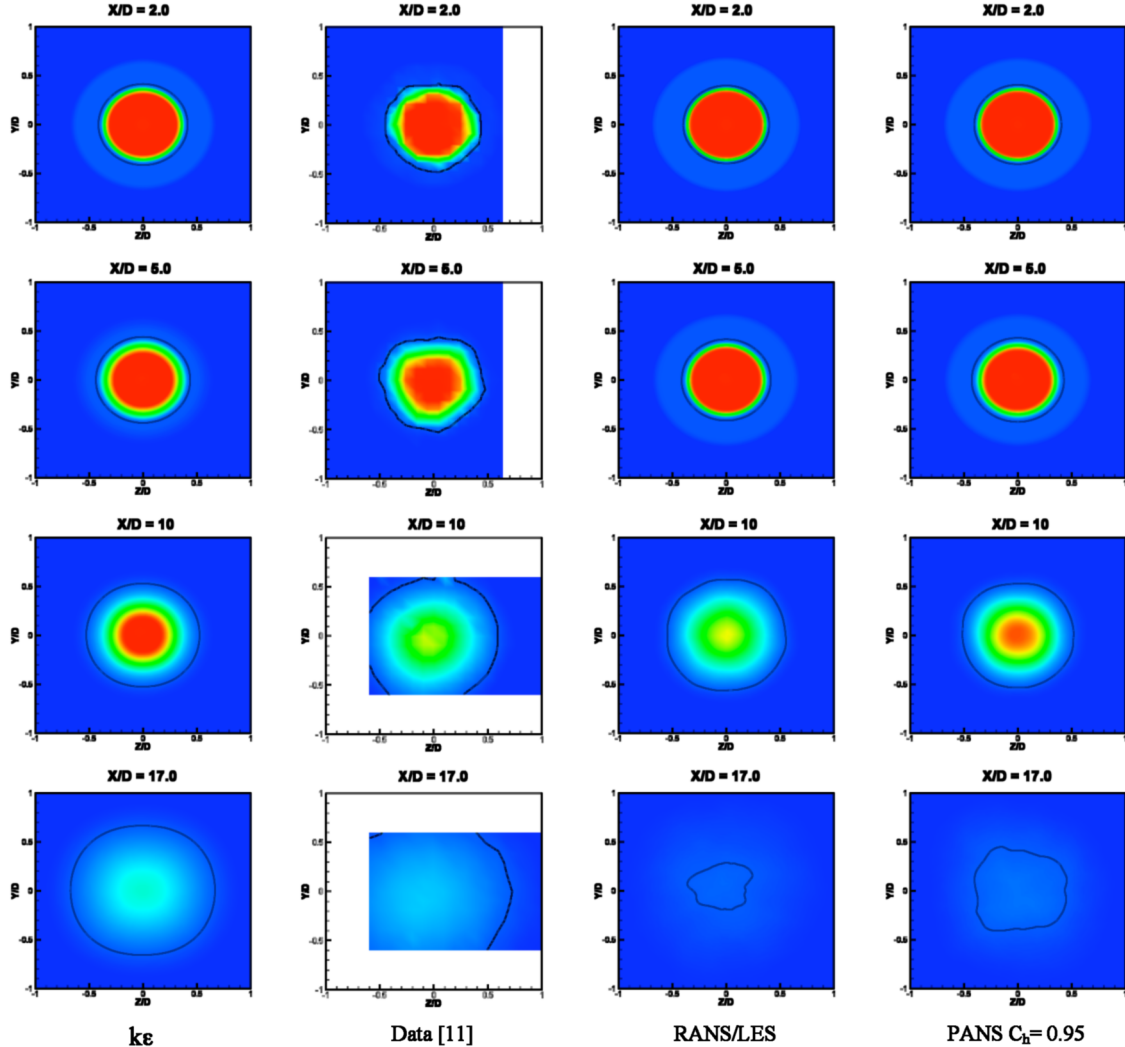

Fig. 12 Comparison of the stagnation temperature prediction with data [10].

coordinate with the data presented in [10]. The computational results were computed for a freestream Mach number of 0.28. For the PANS calculations $C_h = 1.05$ and $C_h = 0.95$ to study the sensitivity of the prediction to the variation of C_h.

Comparisons of computed stagnation temperatures at the symmetry plane show that both RANS/LES and PANS produced faster mixing than the RANS solution, as shown in Fig. 10. Comparisons between computed stagnation temperature and experimental data are shown in Figs. 11 and 12. The RANS solution produces slower mixing than the experimental data. On the other hand, RANS/LES produces better agreement with the data than the RANS results. In Fig. 11, the calculations were compared with the experimental centerline values. We also found that the PANS solutions are sensitive to the variation of C_h. As shown in Fig. 12, RANS/LES was able to more accurately predict the temperature flowfield and produce a result closer to the experimental data, whereas the RANS approach overpredicted the temperature in the core region. The results from PANS were in reasonably good agreement with experimental data.

IV. Conclusions

The hybrid RANS/LES and PANS turbulence models are relatively new and will need to be exercised for a wide variety of problems to determine their accuracy before they become an accepted tool for fluid dynamics modelers. They seem to offer much for unsteady flow applications, but issues such as grid sensitivity need to be further addressed. It is hoped that more effort will go into these models in the near future, so that they can be matured for use in everyday applications. The new capabilities have the potential to improve the accuracy and robustness of creating a simulation of an unsteady flowfield. This new class of turbulence models is inherently grid-size-dependent, because increasing the grid resolution allows smaller and smaller turbulent scales to be resolved.

We have introduced and implemented a novel two-stage procedure to efficiently estimate the level of scale resolution possible for a given flow on a given grid for partially averaged Navier–Stokes (PANS) and other hybrid models. This is a two-stage procedure. In the first stage, a RANS simulation with a standard turbulence model (STM) such as $k\varepsilon$ is used to produce an estimate of f_k over the entire grid domain. In the second stage, we supply f_k for the selective application of a hybrid turbulence model (HTM) such as the PANS formulation in regions in which the grid density is sufficient to resolve a portion or all of the large-scale flow structures. In the present implementation, f_k is a function of length scale and grid size that represents a characteristic length-scale ratio.

In the present paper, we selected the subsonic high-temperature jet flows to calibrate and validate the PANS approach. This implementation was a first step toward adding a variable-resolution turbulence model capability to CFD codes. The PAB3D code can now be used to refine the PANS formulation and to conduct validation computations using a variety of simple and complex flow physics problems. This approach needs to be calibrated, verified, and validated for a wide range of flow problems such as different temperature jet, cavity, and others.

Acknowledgments

References

[1] Spalart, P. R., "Young Person's Guide to Detached Eddy Simulation Grids," NASA CR-2001-211032, 2001.

[2] Nichols, R. H., and Nelson, C. C., "Application of Hybrid RANS/LES Turbulence Models," AIAA Paper 2003-0083, 2003.

[3] Mani, M., and Paynter, C. C., "Hybrid Turbulence Models for Unsteady Simulation of Jet Flows," AIAA Paper 2002-2959, 2002.

[4] Batten, P., Goldberg, U., and Chakravarthy, S., "LNS—An Approach Towards Embedded LES," AIAA Paper 2002-0427, 2002.

[5] Girimaji, S., Sreenivasan, R., and Jeong, E., "PANS Turbulence Model For Seamless Transition Between RANS, LES, Fixed-Point Analysis and Preliminary Results," FEDSM 2003, Honolulu, HI, American Society of Mechanical Engineers, Fluids Engineering Div., Paper 2003-45336, 13–16 July 2003.

[6] Abdol-Hamid, K., "Development of Three-Dimensional Code for the Analysis of Jet Mixing Problem," NASA CR 4200, 1988.

[7] Massey, S. J., and Abdol-Hamid, K. S., "Enhancement and Validation of PAB3D for Unsteady Aerodynamics," AIAA Paper 2003-1235, 2003.

[8] Abdol-Hamid, K., and Girimaji, S., "A Two-Stage Procedure Toward the Efficient Implementation of PANS and Other Hybrid Turbulence Models," NASA TM-2004-213260, 2004.

[9] Seiner, J. M., Ponton, M. K., Jansen, B. J., and Lagen, N. T., "The Effects of Temperature on Supersonic Jet Noise Emission," *Proceedings of the 14th DGLR/AIAA Aeroacoustics Conference*, Vol. 1, A93-19126 05-71, Deutsche Gesellschaft für Luft- und Raumfahrt, Bonn, Germany, 1993, pp. 295–307; also DGLR Paper 92-02-046, May 1992.

[10] Thomas, R. H., Kinzie, K. W., and Pao, S. Paul, "Computational Analysis of a Pylon-Chevron Core Nozzle Interaction," AIAA Paper 2001-2185, May 2001.

[11] Theis, A. T., and Tam, C. K. W., "Computation of Turbulent Axisymmetric and Nonaxisymmetric Jet Flows Using the K-ε Model," *AIAA Journal*, Vol. 34, No. 2, Feb. 1996, pp. 309–316.

[12] Tam, C. K. W., and Ganesan, A., "A Modified k-ε Model for Calculating the Mean Flow and Noise of Hot Jets," AIAA Paper 2003-1064, Jan. 2003.

[13] Lebedev, A. B., Lyubimov, A. D., Maslov, V. P., Mineev, B. I., Secundov, A. N., and Birch, Stanley, F., "The Prediction of Three-Dimensional Jet Flows for Noise Applications," AIAA Paper 2002-2422, 2002.

[14] So, R. M. C., and Sommer, T. P., "An Explicit Algebraic Heat-Flux Model for the Temperature Field," *International Journal of Heat and Mass Transfer*, Vol. 39, No. 3, Feb. 1996, pp. 455–465.
doi:10.1016/0017-9310(95)00157-5

[15] Ronki, M., and Gatski, Thomas, B., "Predicting Turbulent Convective Heat Transfer in Fully Developed Duct Flows," *International Journal of Heat and Fluid Flow*, Vol. 22, No. 4, Aug. 2001, pp. 381–392.
doi:10.1016/S0142-727X(01)00104-7

[16] Abe, K., Kondoh, T., and Nagano, Y., "A Two-Equation Heat Transfer Model Reflecting Second-Moment Closures for Wall and Free Turbulent Flows," *International Journal of Heat and Flow*, Vol. 17, No. 3, June 1996, pp. 228–237.
doi:10.1016/0142-727X(96)00037-9

[17] Abdol-Hamid, K., Pao, S., Massey, S., and Elmiligui, A., "Temperature Corrected Turbulence Model for High Temperature Jet Flow," *Journal of Fluids Engineering*, Vol. 126, No. 5, 2004, pp. 844–850.
doi:10.1115/1.1792266

[18] Bridges, J., and Brown, C., "Parametric Testing on Single Flow Hot Jet," AIAA Paper 2004-2824, 2004.

[19] DeBonis, J., "A Large-Eddy Simulation of a High Reynolds Number Mach 0.9 Jet," AIAA Paper 2004-3025, 2004.

[20] Massey, S. J., Thomas, R. H., Abdol-Hamid, K. S., and Elmiligui, A., "Computational and Experimental Flowfield Analyses of Separate Flow Chevron Nozzles and Pylon Interaction," AIAA Paper 2003-3212, 2003.